Separation and Purification Technology 306 (2023) 122604

Contents lists available at ScienceDirect

Separation and Purification Technology

journal homepage: www.elsevier.com/locate/seppur

Experimental and numerical study of the flux of isobutane vapors near saturation through multi-layered ceramic membranes

Katerina Setnickova [a,*], Roman Petrickovic [a], Petr Uchytil [a], Thomas Loimer [b,*]

[a] Institute of Chemical Process Fundamentals, Academy of Sciences of the Czech Republic, 165 02 Prague, Czech Republic
[b] Institute of Fluid Mechanics and Heat Transfer, TU Wien, 1060 Vienna, Austria

ARTICLE INFO

Keywords:
Mass flow
Inorganic membranes
Porous media
Capillary condensation
Joule–Thomson effect

ABSTRACT

The transport of vapors of isobutane near saturation through multi-layered asymmetric membranes is investigated experimentally and theoretically. The influence of the upstream state of the vapor, whether far or close to saturation, and of the orientation of the membrane on the mass flow rate is investigated. For a membrane with five layers, the mass flux increases from about 0.25 $kg\,m^{-2}s^{-1}$ for a vapor further from saturation to about 0.45 $kg\,m^{-2}s^{-1}$ for a vapor close to saturation. Also, close to saturation the mass flux in the flow direction from the separation layer to the support is up to 50% larger than in the opposite direction. The membranes consist of three to five layers, the support has a pore size of 3 μm, the finest separation layer has a pore size of 20 nm. Plane, circular membranes were tested in steady-state permeation experiments. The upstream pressure varied between about 0.3 times the saturation pressure and a value a few percent smaller than the saturation pressure, which is about 3.5 bar. Pressure differences between 0.1 and 0.5 bar were applied. Theoretical descriptions of the flow process are given, assuming that condensation may take place. For one description any heat transfer is neglected and the flow is assumed to be isothermal while for two other descriptions heat transfer and temperature variations due to condensation and evaporation are considered. For the experiments presented here the mass fluxes predicted by these three descriptions do not differ by a wide margin, e.g., the predictions vary between 1.02 and 1.25 $kg\,m^{-2}s^{-1}$. Qualitatively, the increase of the mass flux for a vapor close to saturation and the dependence of the mass flux on the flow direction is recovered by all three descriptions.

1. Introduction

Inorganic membranes usually consist of several layers, which differ in pore size and thickness. A hierarchy of structural properties often offers advantages, for instance for the combination of pressure drop and mechanical strength [1]. Commonly, a support layer is used, which has a large pore size, large thickness and which provides structural stability. On top of the support layer several intermediate layers with smaller thicknesses and decreasing pore sizes and finally the separation layer with the smallest thickness and smallest pore size is placed. Thus, a membrane consisting of several different layers is mostly asymmetric with respect to the flow direction. The fluid may either flow in the direction from the support to the separation layer, or in the reverse direction from the separation layer to the support.

For instance, tubular ceramic membranes may have the separation layer at the inside or at the outside of the tube, and the feed may be also be applied at the inside or at the outside. It would be of interest, whether the flow direction plays a role in membrane performance. Here, because of availability, plane, not tubular membranes were investigated. While the influence of the flow direction has been investigated for gaseous flow, data and descriptions for flows with condensation are scarce. The present investigation contributes experimental data under these conditions, and highlights the importance of heat transfer and temperature boundary conditions on membrane permeance.

In the following, we recall modeling efforts and results for purely gaseous flow through homogeneous porous media, followed by a recount on the effect of capillary forces for flows with condensation. Condensation and evaporation leads to the treatment of temperature variations and energy transport. Furthermore, it is mentioned that the Joule–Thomson effect may play a role, and different boundary conditions are proposed. At the end of the introduction section, the choice of the experimental method is justified.

* Corresponding authors.
E-mail addresses: setnickova@icpf.cas.cz (K. Setnickova), petrickovic@icpf.cas.cz (R. Petrickovic), uchytil@icpf.cas.cz (P. Uchytil), thomas.loimer@tuwien.ac.at (T. Loimer).

https://doi.org/10.1016/j.seppur.2022.122604
Received 22 September 2022; Received in revised form 28 October 2022; Accepted 6 November 2022
Available online 11 November 2022

The transport of vapors and non-condensable gases through porous membranes can be described, from application of the dusty-gas model [2], as a combination of viscous and molecular flow. Uchytil [3] compared the pore radius obtained from interpreting permeation data as the sum of viscous and molecular flow with the pore radius obtained from mercury porosimetry, and found good agreement. Similarly, the flow of gases through ceramic asymmetric membranes with one and up to five layers was described as the sum of viscous and molecular contributions [4]. The pore size could be recovered from the permeation data, and mass flow differences of up to 6% between the two flow directions for ideal gases were computed [4]. Mass flow differences were also computed for a membrane consisting of two layers [5], and these mass flow differences, of up to 50% depending on the pressure conditions, were experimentally verified [6]. The influence of the transport direction on permeance was also investigated on a stack of two homogeneous membranes, mimicking an asymmetric two-layer membrane [7]. It should be recalled that a description where interactions between fluid molecules and the walls of the porous medium are not taken into account is applicable if the pore size is much larger than a fluid molecule, or if fluid molecules do not interact with the pore walls. However, accounting for these additional transport mechanisms, the importance of the orientation on mass transport was also computed for a two-layer membrane [8] and shown for zeolite membranes [9].

In contrast to gases, a vapor that flows through a porous membrane may condense. The flow of vapors through Vycor glass membranes with pore diameters of 4 nm was described by Rhim & Hwang [10], accounting for viscous, molecular and surface flow and also considering capillary condensation. Rhim & Hwang [10] mentioned that when condensation occurs a large enthalpy of vaporization is transported, and the flow cannot be isothermal. However, an isothermal model was used [10], and later similar experimental data for Vycor glass was described as isothermal flow [11]. With the inclusion of surface flow an effect of pore blocking by condensate could be observed and modeled [12], while other experimental data did not show a maximum in permeance versus mean pressure [13]. For the flow of butane through 4 nm Vycor glass membranes, with an upstream state of either a liquid or a gaseous state, the role of capillary pressure was worked out [14]. Data from steady-state and unsteady permeation experiments for butane through 4 nm Vycor glass membranes was reported [15]. In the references mentioned above, the flow was modeled as isothermal, and the large capillary pressure at the strongly curved interfaces between the liquid and the gaseous phase of the fluid within the porous membrane was taken into account [10–15]. To recover a flow hysteresis, non-equilibrium molecular dynamics simulation or lattice-based dynamic mean field theory should be used [16].

Schneider [17] relaxed the assumption of isothermal flow, considered the balances of mass, momentum and energy and took into account real-gas properties, recovering the Joule–Thomson effect. The flow of propane through a stretched polyethylene membrane with a pore width of 20 nm was measured and could be well described [17]. The same model was applied to a two-dimensional flow through a slender cylinder [18]. A salient feature of the non-isothermal description [17] is that a vapor near saturation that flows through a porous membrane may also condense only due to the Joule–Thomson effect, capillary effects may be disregarded.

Capillary effects were later included in a non-isothermal description of the flow based on the model given by Schneider [17], and a large amount of experimental data was presented [19]. This model was subsequently applied to a theoretical study of the flow of isobutane through an asymmetric membrane consisting of three layers [20]. Depending on the flow direction, from the separation layer to the support or from the support to the separation layer, the mass flux could be up to ten times larger in one direction than in the other direction [20]. A factor of seven was reported in another study [21]. Analyzing the flow of propane through an asymmetric membrane whose properties were given elsewhere [4], mass flux differences, pressure profiles and the distribution of liquid phase in the membrane was given [22].

Here, the description of the flow is refined with respect to heat transfer from the surroundings. Accounting for real-gas properties of the fluid and assuming adiabatic boundary conditions at the upstream and the downstream side of the membrane, the Joule–Thomson effect is recovered. However, due to small mass flow rates through the membrane, the assumption of adiabatic flow may be unrealistic. Therefore, heat transfer from the environment to the membrane is allowed, and the flow is described for (i) purely isothermal flow, (ii) adiabatic boundary conditions, and (iii) a diabatic downstream boundary, i.e., requiring that the downstream temperature of the fluid shall be equal to the upstream temperature. In the latter case, temperature variations within the domain are allowed.

The mass flow of isobutane through asymmetric membranes with up to five layers was measured. Isobutane was chosen because its saturated vapor pressure at a laboratory temperature of 25 °C is 3.51 bar. A pressure in the range between 2 to 5 bar is suitable for experiments for several reasons. During the experiments, a pressure difference can be set that the flow through the studied ceramic membranes is easily measurable. In the case of using a substance with a low pressure such as water, which has a saturated vapor pressure of 0.0312 bar at 25 °C, only a small pressure difference across the membrane could be applied. Hence, the mass flow rate would be small and therefore not precisely measurable. Also, measurement of small values would place additional demands on the tightness of the apparatus. Increasing the pressure of water vapor by increasing the temperature of the experiment would require an extensive heat insulation of the whole apparatus. An elevated temperature and bulky heat insulation would make operation of the apparatus much more inconvenient. Therefore, isobutane was found to be very suitable for investigating mass transport accompanied by condensation in small pores of a membrane.

While experiments were only done with isobutane, the theoretical description and some findings from this study are also applicable to other fluids and asymmetric membranes. However, the minimum pore size is restricted to about 10 nm. Otherwise, fluid–wall interactions should be taken into account, which is not done in the description presented here. There is no maximum pore size beyond which the proposed model would become invalid. However, beyond a pore size of perhaps 500 nm, several terms in the current description, e.g., those relating to molecular flow but also to capillary pressure, become small or even insignificant. Therefore, for flows through media with pore sizes on the order of microns, the proposed description is too complicated, involves terms that do not play a role, and conclusions drawn for flow through asymmetric media may not be applicable.

2. Theory

To describe the ceramic membranes, a model of the porous media as consisting of equivalent, parallel, round capillaries is invoked. The properties of these equivalent porous media are partially determined from permeation experiments with nitrogen, cf. Section 3.1. The inner diameters of these capillaries change discontinuously according to the pore size of the corresponding layer. The contact angle inside the capillaries is assumed to be zero and constant, i.e., independent of the mass transfer across the meniscus. As a consequence, if there is a front of phase change within the capillaries, the curvature of the menisci within the capillaries is uniquely determined by the contact angle and the pore radius. Heat conduction within the ceramic membrane is modeled by treating the membrane as a homogeneous medium, assigning an effective thermal conductivity to the membrane filled with either the liquid or the gaseous phase of the fluid.

In the following, the governing equations are given for three one-dimensional descriptions of the flow through the asymmetric porous membrane, an isothermal, an adiabatic, and a diabatic description: In the first, isothermal description, heat transfer is not taken into

Table 1
Material properties of isobutane and thermal conductivity of the membrane.

Property	Correlation	Ref.
R	$R = \mathcal{R}/\mathcal{M}$, $\mathcal{R} = 8314.4$ J kmol^{-1} K^{-1}, $\mathcal{M} = 58.124$ kg kmol^{-1}	[23]
p_{sat}	$p_{sat} = 10\,\hat{}\left(\left(9.00272 - \frac{947.54}{T/\mathrm{K}-24.28}\right)\left(0.43429\chi^{2.6705} - 19.64\chi^{8} + 2792\chi^{12}\right)\right)$ Pa, $\chi = \frac{T/\mathrm{K}-268}{407.1}$	[24]
v_l	$\rho_l = 870.93 - 1.36494(T/\mathrm{K}) + 0.00256419(T/\mathrm{K})^2 - 5.32743\times^{-6}(T/\mathrm{K})^3$ kg m^{-3}, $v_l = \rho_l^{-1}$	[25]
v_g	$v_g = \frac{\tilde{v}_{id}}{2\mathcal{M}} + \sqrt{\frac{\tilde{v}_{id}^2}{4\mathcal{M}^2} + \frac{B\tilde{v}_{id}}{\mathcal{M}^2}}$, $\tilde{v}_{id} = \frac{RT}{p}$, $B = 0.11625 - \frac{102.93}{T/\mathrm{K}} - \frac{12\,475}{(T/\mathrm{K})^2} - \frac{7.0490\times10^6}{(T/\mathrm{K})^3}$ m^3 kmol^{-1}	[26]
$c_{p,l}$	$\tilde{c}_{p,l} = 172\,370 - 1783.9\frac{T}{\mathrm{K}} + 14.759\left(\frac{T}{\mathrm{K}}\right)^2 - 0.047909\left(\frac{T}{\mathrm{K}}\right)^3 + 5.805\times10^{-5}\left(\frac{T}{\mathrm{K}}\right)^4$ J kmol^{-1} K^{-1} $c_{p,l} = \tilde{c}_{p,l}/\mathcal{M}$	[27]
$c_{p,id}$	$\tilde{c}_{p,id} = 65\,490 + 247\,760\left(\frac{1587/(T/\mathrm{K})}{\sinh(1587/(T/\mathrm{K}))}\right)^2 + 157\,500\left(\frac{706.99/(T/\mathrm{K})}{\cosh(706.99/(T/\mathrm{K}))}\right)^2$, $c_{p,id} = \tilde{c}_{p,id}/\mathcal{M}$	[27]
v_l	$\mu_l = \exp(-18.345 + \frac{1020.3}{T/\mathrm{K}} + 1.0978\ln(T/\mathrm{K}) - 6.1\times10^{-27}(T/\mathrm{K})^{10}$ Pa s, $v_l = \mu_l/\rho_l$	[28]
v_g	$\mu_g = \left(0.807T_r^{0.618} - 0.357e^{-0.449T_r} + 0.34e^{-4.058T_r} + 0.018\right)\sqrt{\mathcal{M}}\left(\frac{408.2R(6.02214\times10^{26})^2}{(3.65\times10^6)^4}\right)^{-1/6}$ Pa s, $T_r = (T/\mathrm{K})/408.2$	[29]
k_l	$k_l = 0.1495(1-T_r)^{0.38}/T_r^{1/6}$ W m^{-1} K^{-1}, $T_r = (T/\mathrm{K})/408.2$	[30]
k_g	$k_g = \frac{8.757(\exp(0.0464T_r)-\exp(-0.2412T_r))+9.55(-0.152T_r+1.191T_r^2-0.039T_r^3)}{0.457\times10^6(408.2\mathcal{M}^3/(3.65\times10^6)^4)^{1/6}}$ W m^{-1} K^{-1}, $T_r = \frac{T/\mathrm{K}}{408.2}$	[31]
σ	$\sigma = 0.0505731(1-(T/\mathrm{K})/408.15)^{1.24412}$ N m^{-1}	[32]
Δh_{vap}	From Clausius–Clapeyron, $\Delta h_{vap} = (\mathrm{dp}_{sat}/\mathrm{dT})T(v_g - v_l)$	
k_m	$k_m = 30$ W m^{-1} K^{-1}	[33]

account, and the flow is assumed to be isothermal throughout the entire flow field. In the second and third descriptions, account is taken of the enthalpy of vaporization released or consumed at fronts of phase change, of heat transfer within the flow, and of the real fluid properties of the fluid. The second and the third description differ only in one boundary condition at the downstream side of the membrane. For the adiabatic description, it is assumed that there is no heat flux to or from the membrane. Hence, the Joule–Thomson effect is recovered: The temperature of the fluid at the downstream side of the membrane is smaller than the temperature at the upstream side of the membrane. Conversely, for the third, the diabatic description, the downstream temperature is assumed to be equal to the upstream temperature. This boundary condition results in a heat flux from the environment to the downstream side of the membrane. In contrast to the isothermal description, there is still a temperature variation within the membrane.

2.1. Governing equations

The balances of mass, momentum and energy are given by [19]

$$J = \text{constant}, \tag{1}$$

$$J = -\frac{\kappa}{\nu}\frac{\mathrm{d}p}{\mathrm{d}z}, \tag{2}$$

$$Jh + \dot{q} = \text{constant}, \tag{3}$$

where J is the mass flux, κ refers to the permeability of the membrane, ν denotes the kinematic viscosity of the fluid, p refers to the pressure, the spatial coordinate in flow direction is given by z, the specific enthalpy of the fluid is given by h and $\dot{q}$ refers to the heat flux. Note, that D'Arcy's equation is used as the momentum balance, and that the kinetic energy of the fluid is neglected in the energy equation. Therefore, this description is restricted to porous media with small pore sizes. Modeling the porous medium as a bundle of parallel capillaries, the permeability is related to the pore radius by [34, p. 128]

$$\kappa = \frac{\epsilon}{\tau}\frac{r^2}{8}, \tag{4}$$

where ϵ is the void fraction, τ the tortuosity, and r is the pore radius. The flow of the gaseous phase through the porous medium is taken to be the sum of viscous and molecular flow, applying a result from the dusty-gas model [2]. Hence, for the gaseous phase an apparent kinematic viscosity can be defined as

$$\nu = \nu_g(1 + \beta Kn)^{-1}, \tag{5}$$

where ν_g is the kinematic viscosity of the gaseous phase in the bulk, β is a correction factor for molecular flow, and Kn is the Knudsen number.

The heat flux $\dot{q}$ is given by Fourier's law of heat conduction,

$$\dot{q} = -k\frac{\mathrm{d}T}{\mathrm{d}z}, \tag{6}$$

where k is the effective thermal conductivity of the fluid-filled membrane and T refers to the absolute temperature. The effective thermal conductivity is computed from the effective medium theory equation [35],

$$k = (1/4)\left((3\epsilon-1)k_f + (2-3\epsilon)k_m + \sqrt{((3\epsilon-1)k_f + (2-3\epsilon)k_m)^2 + 8k_m k_f}\right), \tag{7}$$

with k_f and k_m referring to the thermal conductivity of the fluid and the solid matrix, respectively. Eq. (7) yields the bound between materials where a disperse phase is more conductive than the homogeneous phase, and materials with a homogeneous phase that is higher conductive than the dispersed phase. Ceramic membranes with loosely contacting granules belong to the former. Nevertheless, the data given in Ref. [35] indicates that Eq. (7) gives a good estimate for the effective thermal conductivity of the fluid-filled ceramic membranes utilized here.

At interfaces within the porous medium, the pressure difference across the meniscus is given by the Young–Laplace equation,

$$\Delta p = 2\sigma/r, \tag{8}$$

where σ refers to the surface tension. Eq. (8) above is valid for a contact angle of zero between the liquid phase of the fluid and the solid matrix of the membrane, i.e., for an ideally wetting fluid. The pressure of the gaseous phase of the fluid that is in equilibrium with its liquid phase at a curved meniscus is denoted by p_K, and it is given by Kelvin's equation,

$$\ln\left(\frac{p_K}{p_{sat}}\right) = -\frac{2\sigma}{r}\frac{v_l}{RT}. \tag{9}$$

Here, R is the specific gas constant, p_{sat} refers to the saturation pressure and v_l is the specific volume of the liquid phase of the fluid.

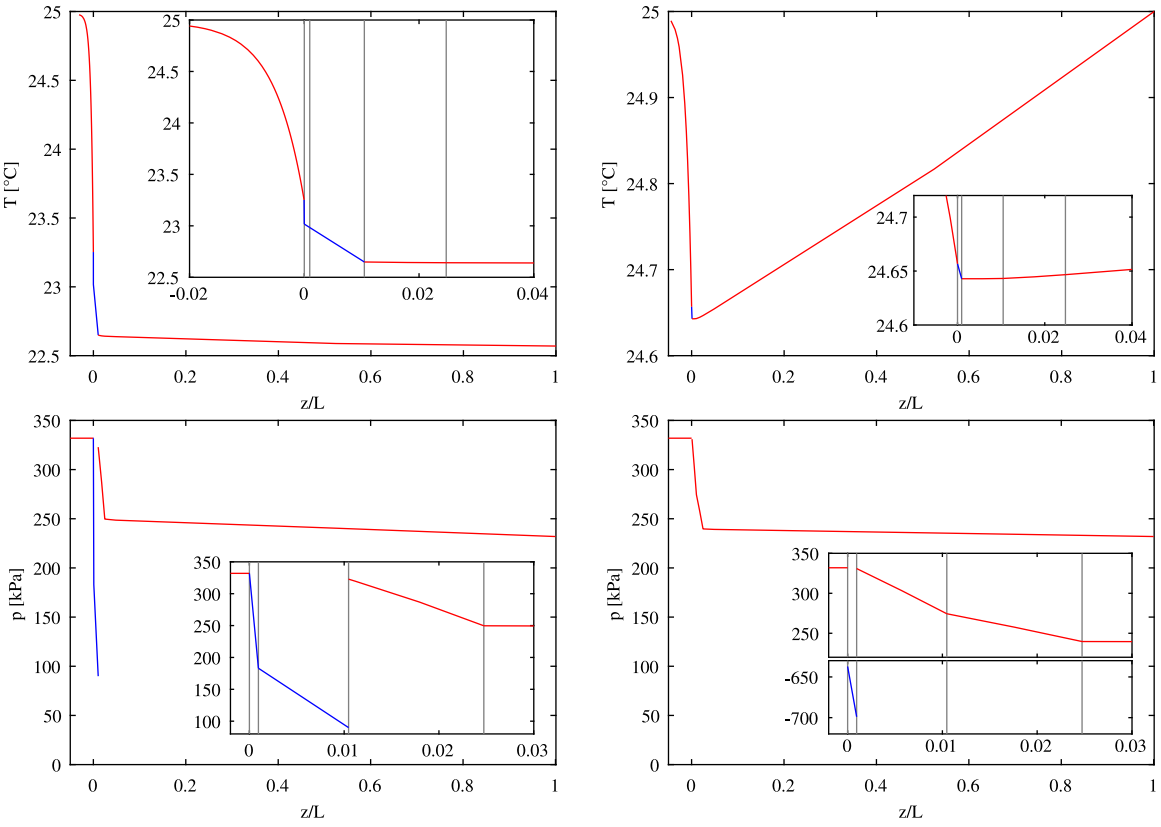

Fig. 1. Temperature (top) and pressure distributions (bottom) according to the adiabatic (left) and the diabatic (right) description. Computed for the flow of isobutane through the membrane with five layers. In both cases, $T_1 = 25$ °C, $p_1/p_{sat} = 0.95$ ($p_1 = 332$ kPa) and $p_1 - p_2 = 100$ kPa. Flow is from the left to the right, direction separation layer – support. Liquid is indicated by blue color, vapor by red color. The insets show enlarged views. Vertical lines in the insets mark the boundaries between layers. A mass flux of 1.66 kg m^{-2} s^{-1} is obtained for the adiabatic description and 0.70 kg m^{-2} s^{-1} for the diabatic description.

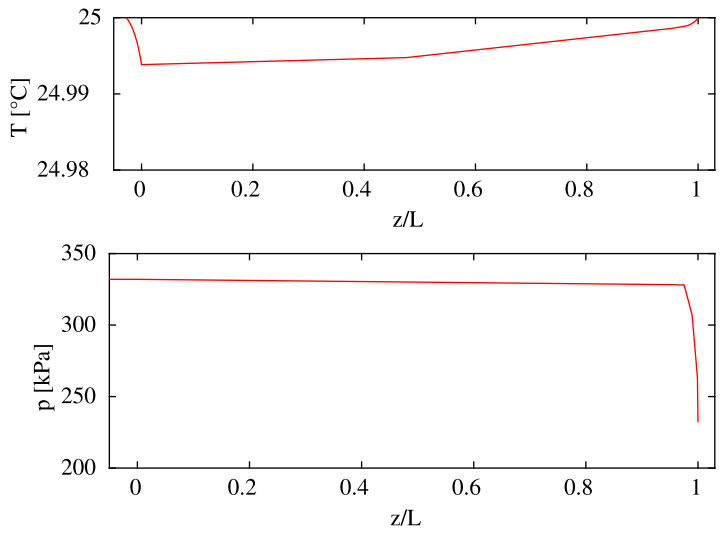

Fig. 2. Temperature and pressure distribution according to the diabatic description for the flow of isobutane in direction support – separation layer through the membrane with five layers, $T_1 = 25$ °C, $p_1/p_{sat} = 0.95$, $p_1 - p_2 = 100$ kPa. The mass flux is 0.515 kg m^{-2} s^{-1}.

At the upstream front of the membrane, the vapor must condense if the upstream pressure is larger than the pressure p_K given by Eq. (9). In that case, Eq. (9) yields the radius of curvature of the meniscus by setting p_K equal to the upstream pressure and solving for r, which in that case denotes the radius of curvature of the meniscus, not the radius of the capillary. A similar situation occurs at the downstream front of the membrane, or at the interfaces between layers with different pore sizes. In the region with the smaller pore size, it must be checked whether the pressure is larger than p_K given by Eq. (9). If so, a front of phase change is located at that position, and the radius of curvature of the meniscus is computed from Eq. (9).

At curved interfaces, the enthalpy of vaporization is different from the enthalpy of vaporization at a plane interface,

$$\Delta h_{vap,K} = \Delta h_{vap} + (p_K - p_{sat})\left(\frac{\partial h_g}{\partial p}\right) - \left(p_K - p_{sat} - \frac{2\sigma}{r}\right)\left(\frac{\partial h_l}{\partial p}\right), \qquad (10)$$

Table 2
Properties of the ceramic membranes.

Layer	Thickness (μm)	Pore diameter (nm)	Porosity	Tortuosity	β
1	1000	3070	0.5	1.2	6
2	25	1840	0.5	1.2	6
3	15	3230	0.5	2.5	1.7
4	10	80	0.3	1.1	11
5	1	20	0.3	1.1	11

Table 3
Open areas of the membrane samples after being glued into the membrane holder with epoxy resin, and equivalent diameter.

Layers	Area (mm^2)	$2\times\sqrt{area/\pi}$ (mm)
3	25.8	5.73
4	34.6	6.64
5	39.1	7.06

where $\Delta h_{vap,K}$ is the enthalpy of vaporization at a curved interface, and Δh_{vap} is the enthalpy of vaporization at a plane interface.

The governing equations are further supplemented by the thermic and caloric equations of state. Correlations for the material properties of the fluid depending on its state and the thermal conductivity of the membrane material are given in Table 1.

2.1.1. Isothermal description

The isothermal description is based on the assumption that the temperature is the same everywhere within the flow field. Hence, the energy balance and equations related to heat flux are not taken into account. The solution according to the isothermal description is calculated from Eqs. (1), (2), (4), (5), (8) and (9).

The boundary conditions are given by the upstream and the downstream pressure,

$$p(z=0)=p_1, \tag{11}$$

$$p(z=L)=p_2. \tag{12}$$

Here, p_1 is the upstream pressure, p_2 is the downstream pressure and L refers to the thickness of the membrane.

2.1.2. Descriptions with heat transfer

In the case that the energy balance is taken into account, the full governing system of equations, Eqs. (1) to (10), must be considered. Under adiabatic conditions, the boundary conditions are given by

$$p(z=0)=p_1, \quad T(z\to-\infty)=T_1, \quad \dot{q}(z\to-\infty)=0, \tag{13}$$

$$p(z=L)=p_2, \quad \dot{q}(z=L)=0. \tag{14}$$

The boundary conditions must partially be applied at negative infinity, to account for a probable temperature boundary layer upstream of the membrane. Under adiabatic conditions, the governing equations and boundary conditions describe a Joule–Thomson process. The downstream temperature can be computed by integrating the Joule–Thomson coefficient along an isenthalpic line

$$T_1 - T_2 = \int_{p_2}^{p_1} \mu_{JT}\,\mathrm{d}p, \tag{15}$$

where $\mu_{JT}=(\partial T/\partial p)_h$ is the Joule–Thomson coefficient. Vapors always have a positive Joule–Thomson coefficient, therefore, the downstream temperature for the flow of a vapor through a porous membrane is always smaller than the upstream temperature.

The porous membranes investigated here have such small pore sizes that the mass flow through the membranes is very small. Therefore, the assumption of adiabatic flow may not be appropriate. Just a small heat flux from the outside may suffice to render the flow not adiabatic. Therefore, for the diabatic description, the assumption of adiabatic flow is relaxed, and it is assumed that the downstream temperature is equal to the upstream temperature. A heat flux from downstreams of the membrane towards the downstream front of the membrane must be imposed to fulfill the boundary condition to the temperature at the downstream front. The diabatic description is equivalent to keeping the membrane in an isothermal environment and having an infinite heat transfer coefficient at the downstream side of the membrane. The boundary conditions for the diabatic description are

$$p(z=0)=p_1, \quad T(z\to-\infty)=T_1, \quad \dot{q}(z\to-\infty)=0, \tag{16}$$

$$p(z=L)=p_2, \quad T(z=L)=T_1. \tag{17}$$

In fact, for numerical integration, from $\mathrm{d}h = (\partial h/\partial p)_T\,\mathrm{d}p$ first the enthalpy difference $h_1 - h_2$ is computed. The downstream heat flux is then set to $\dot{q}_2 = J(h_1 - h_2)$, thus completing the initial value problem starting from $z = L$.

For all descriptions, the corresponding system of equations is solved numerically using a Matlab [36] program. The governing equations are integrated using a shooting method, but marching upstreams against the flow direction. First the downstream state is calculated from the global energy balance,

$$Jh_1 = Jh_2 + \dot{q}_2. \tag{18}$$

The governing equations are then integrated beginning with the downstream state, varying the mass flux J. The solution is obtained when the pressure at $z = 0$ is equal to p_1 within a tolerance of $(p_1 - p_2)/1000$.

2.2. Properties of the descriptions

Temperature and pressure distributions according to the adiabatic and the diabatic description are shown in Fig. 1. At the top, the temperature distributions are plotted. The temperature distribution for the adiabatic description, especially in the enlarged inlet, nicely displays the upstream temperature boundary layer and the kinks in the temperature distribution between regions of liquid and vapor flow, due to consumption and release of the enthalpy of vaporization. The most striking difference between the two temperature distributions is the effect of the downstream boundary condition. The temperature distribution on the left with the adiabatic boundary condition becomes horizontal at $z/L = 1$, indicating zero heat flux, while there is a heat flux in upstream direction over nearly the entire membrane for the diabatic boundary condition on the right. Also, the minimum temperature is much smaller for the adiabatic boundary condition, slightly above 22.5 °C versus 24.6 °C. The lower temperature causes condensation in a larger part of the flow domain for the adiabatic boundary condition, which is better seen in the inlays to the pressure distribution on the bottom of Fig. 1.

The discontinuity in the pressure distribution between the second and third layer on the left, for the adiabatic boundary condition, corresponds to the pressure difference across a curved interface between liquid and gaseous flow that forms within the membrane. This pressure difference acts, in addition to the pressure difference applied between the feed and the permeate side of the membrane, to enhance the mass flow rate. In contrast to the pressure discontinuity within the membrane, the pressure distribution is continuous at the interface between liquid and gaseous flow at the upstream side of the membrane, at $z/L \approx 0$. This continuous pressure distribution indicates that a thin liquid film with a plane interface forms at the upstream side of the membrane. In comparison, for the diabatic boundary condition on the bottom right of Fig. 1, there are pressure discontinuities both at the upstream and the downstream end of the liquid flow region, corresponding to curved interfaces at both sides. The interface form in the first layer with the smallest pores, hence the pressure differences across the interfaces are much larger than in the case of the adiabatic

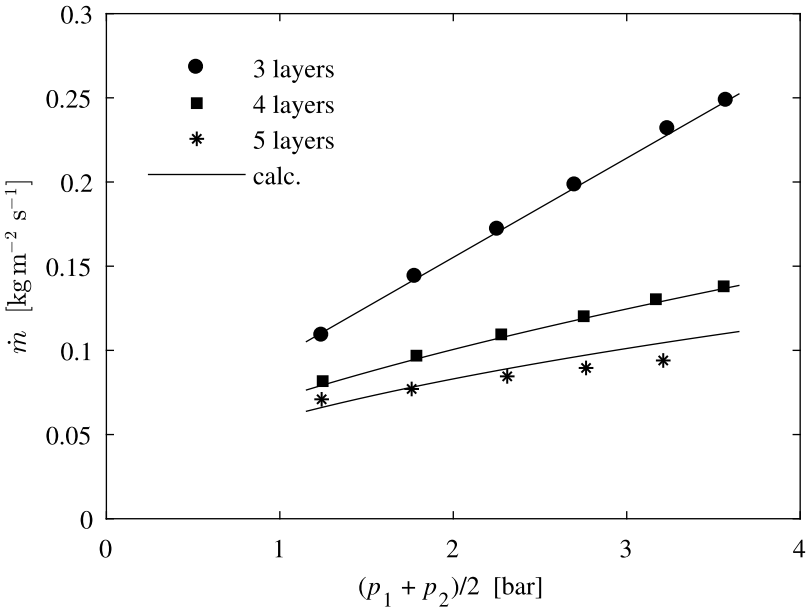

Fig. 3. Mass flux of nitrogen through ceramic membranes with three, four or five layers. The experimental data is used to fit the values of tortuosity and the molecular flow correction factor β. Curves computed from the description with $T_1 = T_2$ and using the fitted values of τ and β are shown as lines.

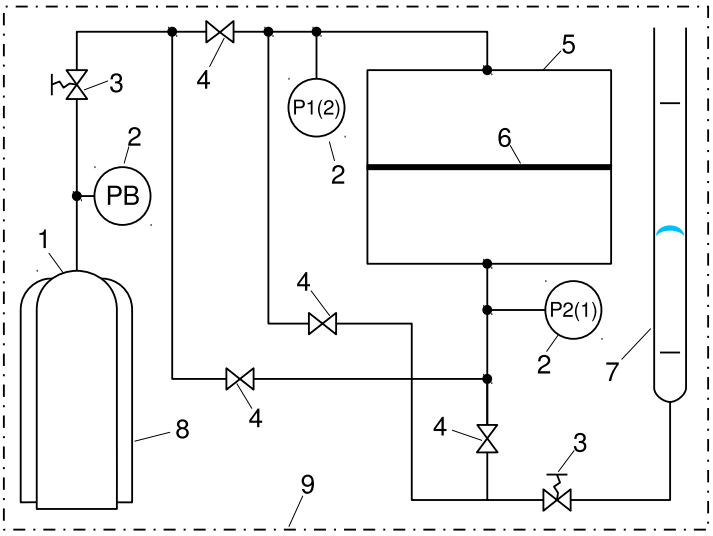

Fig. 4. Flow chart of the experimental apparatus. 1 — gas cylinder, 2 — pressure gauge, 3 — regulating valves, 4 — on/off valves, 5 — permeation cell, 6 — membrane, 7 — bubble flow meter, 8 — heating jacket, 9 — thermostat.

boundary condition, with an interface in the second layer. However, these large pressure differences are nearly balanced, and a net pressure difference across the liquid flow domain of around 100 kPa remains. For the adiabatic description, the pressure difference across the liquid flow domain amounts to a bit more than 200 kPa. Accordingly, the computed mass flux is 1.66 kg m^{-2} s^{-1} in this case with the adiabatic boundary condition and 0.70 kg m^{-2} s^{-1} with the diabatic boundary condition.

For the same conditions as in Fig. 1 on the right the pressure distribution has also been calculated for the reverse flow direction, from the support to the separation layer, see Fig. 2. The layers with the small pores are now on the downstream side of the membrane, where the pressure is lower. Therefore, in contrast to the orientation of the membrane with the small pores on the upstream side, condensation does not occur. The temperature variation is an order of magnitude smaller than with condensation. The mass flow is not enhanced by capillary pressure, the mass flux for this case is 0.52 kg m^{-2} s^{-1}. Hence, we have the result that in this case the mass flux for the two flow directions differs considerably. Without presenting more details, the importance of capillary pressure and the different temperature and pressure conditions in the layers with small pore sizes may suggest why the mass fluxes are different for the two flow orientations if condensation occurs. The above cases were computed for $p_1/p_{sat} = 0.95$. For smaller upstream pressures, condensation does not occur, and there are only small effects of different kinematic viscosities due to different pressures in the individual layers. Hence, without condensation, mass fluxes for different membrane orientations are very similar.

3. Experimental

3.1. Membranes

The membrane samples investigated here correspond to asymmetric membranes at consecutive stages of production. Membrane samples

consisting of only the support layer, of the support layer and the first intermediate layer, of the support layer and two intermediate layers, and so on were produced (Fraunhofer Institut für Keramische Technologien und Systeme, Hermsdorf, Germany). The support layer and the three intermediate layers were made from α-aluminumoxide, the separation layer was made from titaniumoxide.

A plane sample geometry was used, since this is a common shape for membranes, and an apparatus for plane membranes was available. There were no requirements on the chemical composition of the membrane material, other than it should be wetted by the liquid phase of the fluid. A very common material for inorganic porous membranes is α-aluminumoxide, but for very small pore sizes either γ-aluminum or titaniumoxide should be used [37]. The pore size of the separation layer was required to be in the range from about 10 to 50 nm. A previous study has shown that the effect of condensation, i.e., the ratio of the mass flow rate for $p_1 = p_{sat}$ versus the mass flow rate for $p_1 \ll p_{sat}$, increases with decreasing pore size [19]. The larger the pore size, the smaller the ratio of the mass flow rates. According to an adiabatic description of the flow, a critical permeability exists above of which the fluid does not condense completely, and an increased mass transfer due to condensation cannot be observed [19]. For the materials considered here, the critical permeability corresponds to pore sizes of 220 nm for α-aluminum and 420 nm for titaniumoxide. For pores sizes smaller than about 10 nm fluid–wall interaction effects, e.g., surface flow, would start to play a role. These fluid–wall interaction effects are not taken into account in the descriptions presented here, hence a pore size of about 10 nm is regarded as the lower limit or our theoretical descriptions.

The thicknesses, pore sizes and porosities of the individual layers were provided by the manufacturer. The thickness of every layer was measured on the cross section of finished membranes using field emission scanning microscopy, the last, thinnest layer in addition was investigated with transmission electron microscopy on lamella produced with focused ion-beam and on ion-beam etched samples. Pore sizes of the support and the intermediate layers down to 100 nm pore size were measured by mercury porosimetry, the smaller pore sizes were measured by nitrogen sorption technology. The samples to determine pore sizes were produced by spreading small amounts of the respective coating solutions on a polymeric foil, drying, removing the samples from the foil and firing them together with the membranes. The pore size of the 20 nm layer was additionally checked by retention measurement with molecules of known dimensions.

The tortuosity and the molecular flow correction factor β were determined in our laboratory from permeation experiments with nitrogen. The measurements were done with the same experimental setup that was used for the permeation experiments with isobutane, see further below. The mass flux was measured for a pressure difference of approximately 0.4 bar and for different mean pressures. The tortuosity and the molecular flow correction factor β were determined by fitting the expression for the mass flux of a gas through a membrane,

$$J = -\frac{\epsilon}{\tau}\left(\nu_g + \beta \mathrm{Kn}\right)\frac{\mathrm{d}p}{\mathrm{d}z}, \tag{19}$$

to the measured data. Eq. (19) is obtained by substituting the expression for the apparent kinematic viscosity of a gas, Eq. (5), into Eq. (2). Experimental data for the flow of nitrogen through membranes with three, four and five layers and the curves obtained by evaluating Eq. (19) with the values given in Table 2 are shown in Fig. 3. The data for nitrogen transport shown in Fig. 3 was measured in the direction from the smaller pores to the larger pores, i.e., in the flow direction from the separation layer to the support. However, for a gas, the fluxes in opposite flow directions practically do not differ.

Applying a result from the dusty gas model [2] for molecular flow through round tubes yields a value of $\beta = 9.1$, see [22]. The values for β obtained here, with the exception of the value for the third layer, are in the vicinity of this value.

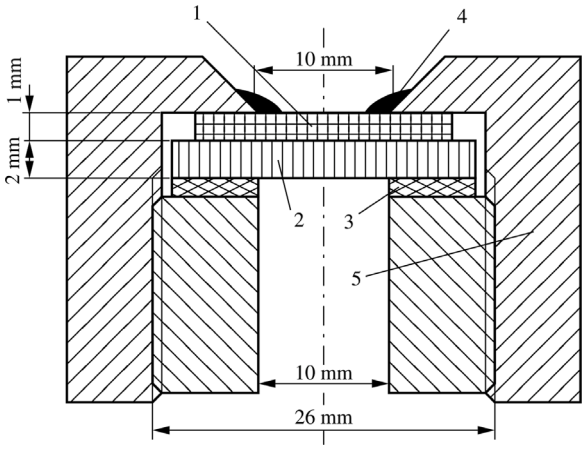

Fig. 5. Membrane holder. 1 — ceramic membrane, 2 — porous glass support, 3 — sealing pad, 4 — epoxy glue, 5 — PVC body.

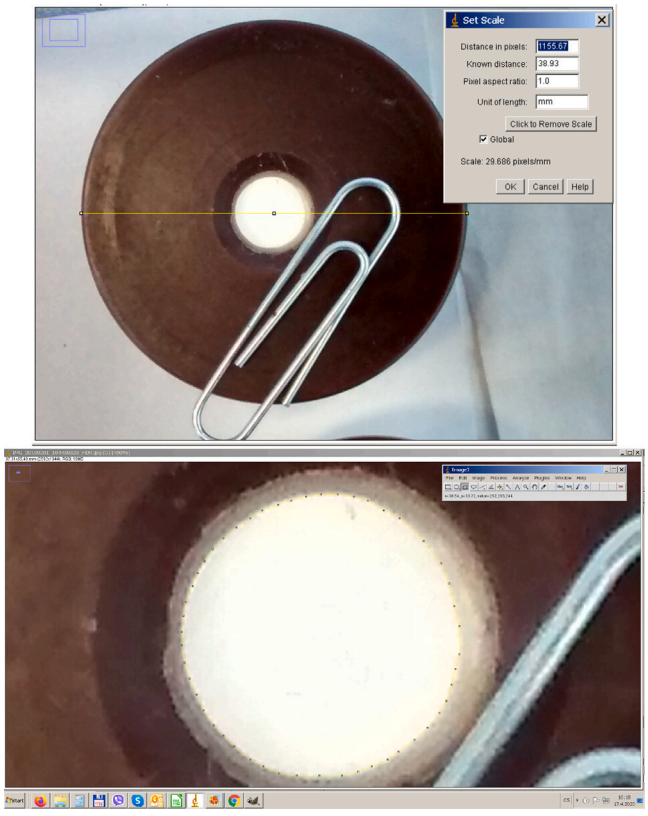

Fig. 6. Photographic image of the membrane holder (top) and an example of the evaluation of the membrane area using the ImageJ [38] software (bottom).

3.2. Experimental setup

A flow chart of the experimental setup is shown in Fig. 4. A permeation cell made from polyvinyl chloride was manufactured in the workshop. Polyvinylchloride is a readily available material that can be easily machined and it thermally insulates the membrane a bit from the surroundings. The permeation cell is connected on one side to a bottle containing isobutane, on the other side it is connected to a bubble flow meter. From the bubble flow meter, the gas exhausts to the atmosphere. On both sides of the permeation cell, pressure gauges and regulating valves (Brooks Instruments, Hatfield, USA) are utilized to maintain constant pressures. Additional shut-off valves and tubing

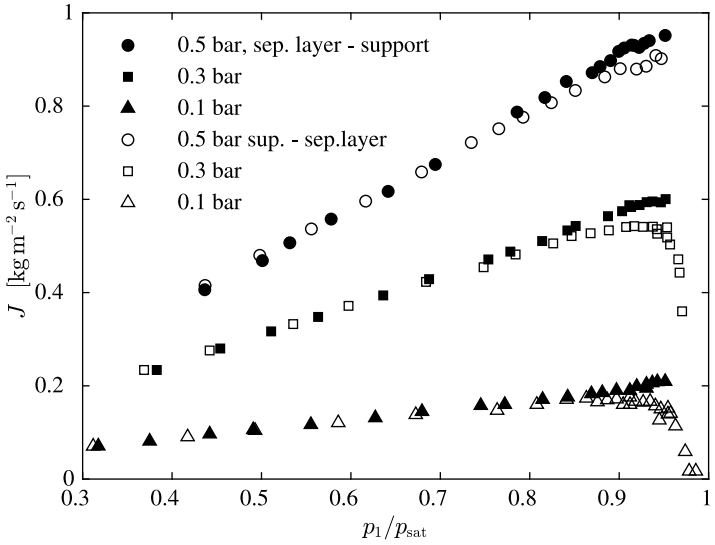

Fig. 7. Mass flux for the flow of isobutane through the membrane with three layers at pressure differences of 0.5, 0.3 and 0.1 bar. Flow direction separation layer – support (filled symbols) and support – separation layer (open symbols).

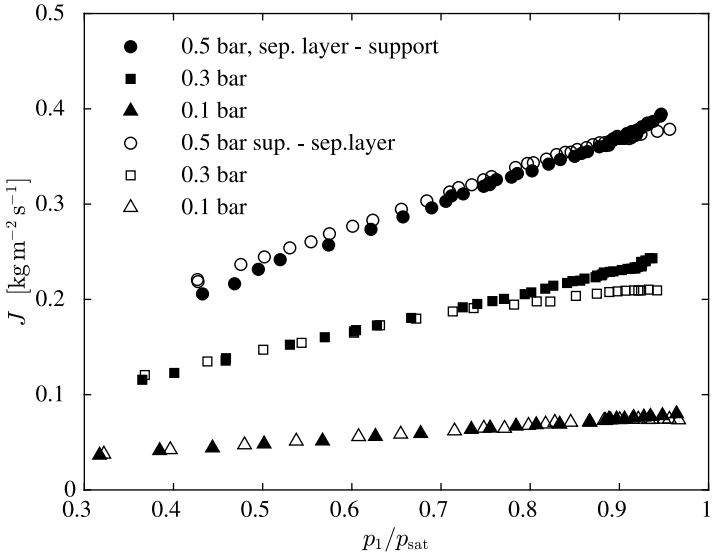

Fig. 8. Mass flux for the flow of isobutane through the membrane with four layers at pressure differences of 0.5, 0.3 and 0.1 bar. Flow direction separation layer – support (filled symbols) and support – separation layer (open symbols).

allow to direct the flow in both directions through the permeation cell. The isobutane bottle is wrapped in a heating jacket connected to a thermostat, and the temperature of the water circulating through the heating jacked is kept constant.

The membrane samples are inserted into the permeation cell by using membrane holders. A membrane sample is fastened with epoxy resin to a circular membrane holder, see Fig. 5. The sample is placed on top of a support made of porous glass S0, which has a thickness of 2 mm and a pore size between 150 and 250 μm. For each membrane sample, the free area is measured by taking a photograph from above the top side of the membrane. The area not obstructed by epoxy resin is determined from the photograph using the image processing software ImageJ [38], see Fig. 6. Table 3 reports the areas measured for the individual membrane samples.

3.3. Measurements

After concluding the experimental setup, initially all the valves, including the regulating valves, are closed. A flow direction is set by opening two of the four block valves. Mass flow data is then taken by first opening fully the regulating valve at the downstream side of the permeation cell. The pressure level in the permeation cell is thus at atmospheric pressure. Next, the regulating valve at the upstream side is carefully opened until the pressure difference between the upstream and the downstream side is approximately at the target value. The pressure level on both sides of the permeation cell is then increased by slowly closing the downstream regulating valve. To keep the pressure difference at the target value, the upstream regulating valve may need to get adjusted. In the procedure above, it is important that initially the downstream valve is fully open. Otherwise, if the upstream valve is first opened, a large pressure difference between the upstream and the downstream side of the membrane may build up, and destroy the membrane.

After adjustments to the regulating valves, a time of five to ten minutes is allowed to pass before a mass flow measurement is taken. For the next measurement, the downstream valve is throttled a bit more, thus raising the pressure level. A series of measurements for a specific pressure difference starts at small pressure levels, increasing

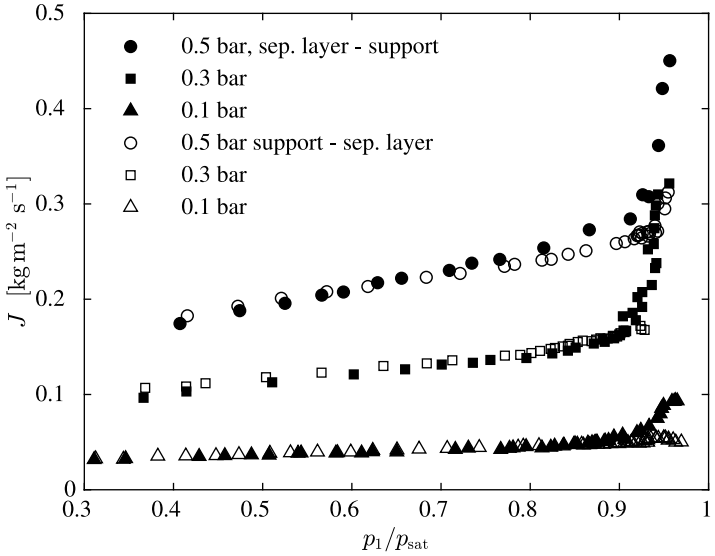

Fig. 9. Mass flux for the flow of isobutane through the membrane with five layers at pressure differences of 0.5, 0.3 and 0.1 bar. Flow direction separation layer – support (filled symbols) and support – separation layer (open symbols).

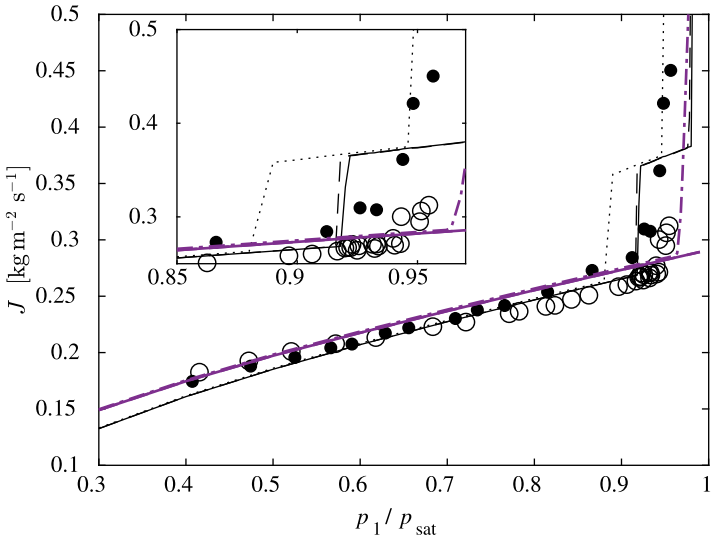

Fig. 10. Mass flux for a pressure difference of 50 kPa, membrane with five layers. Experimental data is denoted by symbols, flow direction separation layer – support (filled circles) and support – separation layer (open circles). Isothermal description (solid line), diabatic description (dashed line) and adiabatic description (dotted line). Computations for the flow direction support – separation layer are shown as thick purple lines.

the pressure level for subsequent measurements. The mass flow rate is calculated from a reading of the bubble flow meter, and noting the atmospheric pressure and the room temperature. For the flow of nitrogen, the measured volumes ranged from 100 ml to 250 ml, for which between 30 to 70 s elapsed. For the flow of isobutane, the measured volumes were mostly between 50 to 100 ml, except for the pressure difference of 0.1 bar, where the measured volumes ranged from 20 to 50 ml. The times it took to fill these volumes lied between a minimum of 12 s, up to 60 s, with a mean of 30 s. The mass flux is calculated from

$$J = \frac{V p_{\mathrm{room}}}{t A R T_{\mathrm{room}}}, \tag{20}$$

where V refers to the measured volume, t to the elapsed time, A is the open area of the membrane, and p_{room} and T_{room} refer to the ambient pressure and temperature, respectively. Here, but not in the numerical computations to calculate the flow field within the membrane, the density of the fluid is evaluated from the ideal gas law.

For measurements where the upstream pressure approached the saturation pressure, the mass flow increased to such large values that the temperature of the bottle could not kept constant any longer. Thus, measurements with the upstream pressure in close vicinity to the saturation pressure were not possible.

4. Results

Mass flow data for the flow of isobutane through membrane samples with three, four and five layers are shown in Figs. 7, 8 and 9, respectively. Flow in the direction from separation layer to the support is indicated by filled symbols, while open symbols stand for the reverse flow direction from the support to the separation layer. Since the minimum pore size decreases and the thickness of the membranes increases slightly with each additional layer, the flow resistance increases with each additional layer. Therefore, as can be seen, the mass flux decreases from Figs. 7 to 9.

A striking feature of the flow data depicted in Fig. 7 is the decrease of the mass flux for p_1 approaching p_{sat} and for the flow direction

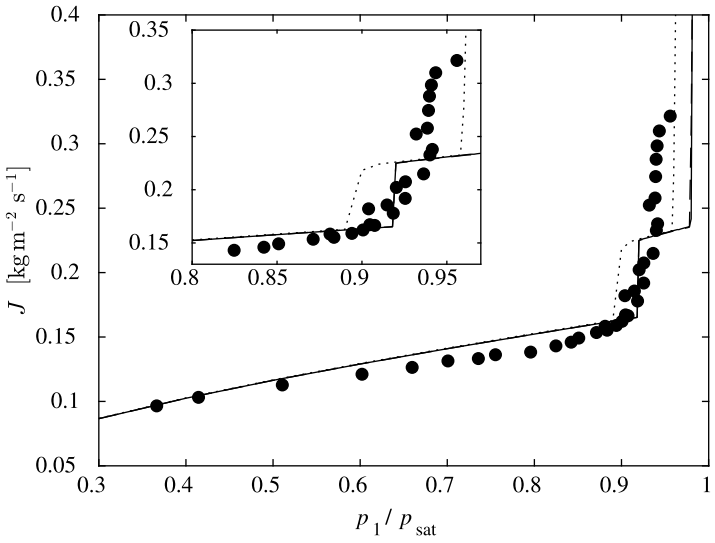

Fig. 11. Mass flux for a pressure difference of 30 kPa, five layers, flow direction separation layer–support. For caption, see Fig. 10. The curves for the isothermal description (solid line) and the diabatic description (dashed line) nearly coincide.

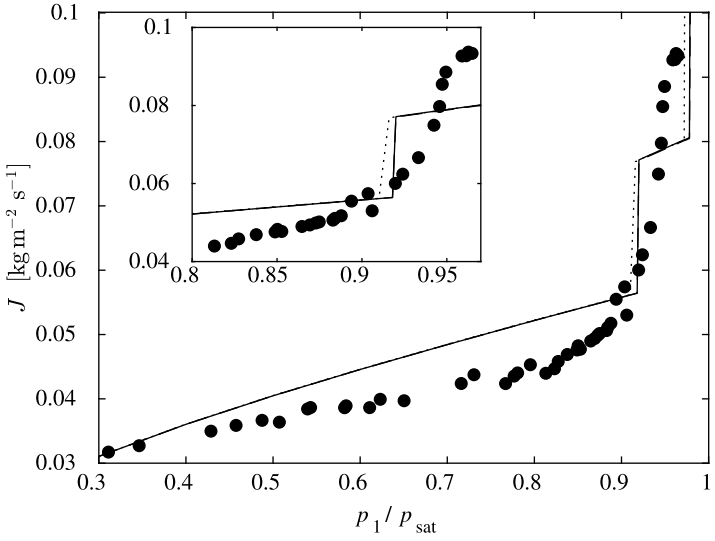

Fig. 12. Mass flux for a pressure difference of 10 kPa, five layers, flow direction separation layer – support. For caption, see Fig. 10. The three descriptions yield nearly the same result.

from the support to the separation layer. This decrease might be caused by contact angle hysteresis and the formation of condensate in the downstream-most layer. This hypothesis is supported by the observation that the decrease of the mass flux only happens at small pressure differences, not at a pressure difference of 0.5 bar. However, a decrease of the mass flux is not seen in the membranes with four or five layers, where the separation layer has smaller pore sizes. On one hand, in smaller, smooth pores a smaller contact angle hysteresis would suffice to form a liquid plug that is able to withstand a given pressure difference. On the other hand, in smaller pores capillary pressure is more dominant, responding less to outer pressure conditions. Nevertheless, there is no good explanation for a decrease of the mass flux for three layers only. This might serve as reminder that modeling the pores as smooth capillaries might lose some properties of the pore space.

Another feature of the mass flow data is that for a vapor far from saturation, the mass flow is independent of the flow direction. As can be seen in Figs. 7 to 9, for p_1 smaller than $\approx 0.9 p_{sat}$, the open and the filled symbols closely coincide. The near independence of mass flow rates on membrane orientation for vapors far from saturation is also reproduced by the theoretical descriptions, see Fig. 10. The theoretical lines shown in Fig. 10 for the two flow directions differ by less than five percent.

The mass flow through the membrane with four layers, Fig. 8, is only slightly larger than the mass flow through the membrane with five layers, Fig. 9. The flow resistance of the fifth layer is small. However, in the region of condensing flow, for $p_1/p_{sat} > 0.9$, due to the action of capillary forces the mass flux through the membrane with five layers, Fig. 9, can become even larger than the mass flux through the membrane with four layers, Fig. 8.

The mass flow data for the membrane with five layers, Fig. 9, shows a strong increase of the mass flow for $p_1/p_{sat} > 0.9$ in the flow direction from separation layer to support. For a pressure difference of 0.5 bar, there is also an increase for the flow direction support-separation layer for $p_1/p_{sat} > 0.9$. The strong increase of the mass flux for upstream states close to saturation is further investigated and compared to predictions from the theoretical descriptions in Figs. 10 to 12.

Fig. 10 shows experimental data and computations for the mass flow through the membrane with five layers for a pressure difference of 0.5 bar. The experimental data shows a sudden increase of the mass flow at $p_1/p_{sat} \approx 0.9$. The isothermal and the diabatic descriptions of the flow also yield a sudden increase of the mass flow at the same

position while, according to the adiabatic description, the mass flow should increase already for smaller values of p_1/p_{sat}. The kinks in the theoretical descriptions are caused by the coarse description of the pore space. The pore diameter changes instantly at the layer boundaries. A gradual change of the pore diameter from one layer to the next would be more realistic.

The maximum mass flow rates according to the theoretical descriptions, which occur for a vapor at saturation upstream of the membrane, $p_1/p_{sat} = 1$, are not shown in Fig. 10. They are $J = 1.19$ kg m^{-2} s^{-1} according to the isothermal description, 1.02 kg m^{-2} s^{-1} according to the diabatic description and 1.25 kg m^{-2} s^{-1} according to the adiabatic description. These values are much beyond the range of mass fluxes shown in the graph, but do not differ widely between themselves.

In the reverse flow direction, from the support to the separation layer, the experimental data seems to show a sudden increase of the mass flow at $p_1/p_{sat} \approx 0.94$. The adiabatic description predicts an increase of the mass flux at nearly the same location. There is no increase of the mass flux according to the diabatic and the isothermal description. Since the sudden increase of mass flow rates depending on the flow direction occurs at different states of the upstream fluid, $p_1/psat \approx 0.9$ versus $p_1/p_{sat} \approx 0.94$, for a vapor close to saturation the mass flow rates through a membrane may differ considerably for the two flow directions.

The smaller the pressure difference across the membrane, the closer the three descriptions of the flow become, see Figs. 11 and 12. For very small pressure differences, the state of the fluid in the upstream part of the membrane does not differ much from the state of the fluid in the downstream part of the membrane. Hence, the smaller the pressure difference becomes a change of the orientation should yield a smaller influence on the mass flow rate. The experimental data shows a much more gradual increase of the mass flow rate than the theoretical predictions. As for the case with a pressure difference of 0.5 bar, the comparison of experimental data with predictions is not much more favorable for one of the descriptions over the others.

5. Conclusions

For isobutane vapors in a state far from saturation and up to $p_1/p_{sat} = 0.9$, the mass flow through the asymmetric ceramic membranes tested here can very well be predicted by any of the descriptions presented here, isothermal, adiabatic, or diabatic. As long as there is no condensation within the flow, there is not much difference between the models. Also, a different orientation of the membrane with respect to the flow direction influences the mass flow rate by less than a few percent. Specifically, a simple isothermal description of the flow, for which the energy balance is not taken into account, yields the same results as more involved descriptions of the flow.

For isobutane vapor close to saturation, the theoretical descriptions predict the formation of condensate in parts of the membrane. The formation of condensate and the pressure profile resulting from the pressure differences across the boundaries between the liquid and the gaseous phase cause a sudden and distinctive increase of the mass flux. A sudden increase of the mass flux for a vapor close to saturation is also seen in the experimental data. In one specific case, due to condensation the mass flux through a membrane with larger resistance could become larger than the mass flux through a membrane with smaller resistance, cf. Figs. 8 and 9. In another case, the mass flux through the membrane in one direction could become approx. 50% larger than the mass flux in the other direction, cf. Fig. 10. The dependency of the mass flux on vapor upstream pressure supports the theory that condensate forms in the membrane.

The comparison of the data with three different descriptions of the flow, one isothermal description for which temperature variations and transport of heat is neglected, and two non-isothermal descriptions, a diabatic and an adiabatic descriptions, does not show clearly whether one of the descriptions should be favored. For an appreciable pressure drop of 0.5 bar, all descriptions show satisfying agreement with the data. For the flow through membranes with three layers and a smallest pore size of 0.23 μm, a decrease of the flow for a vapor close to saturation is not predicted by any of the descriptions.

The modeling of the pore space as consisting of layers with distinctive pore radii that changes discontinuously between layers introduces artifacts, kinks in the distribution of mass flux over upstream pressure. The descriptions should be improved in that respect.

CRediT authorship contribution statement

Katerina Setnickova: Investigation, Validation, Writing – original draft. **Roman Petrickovic:** Investigation, Resources. **Petr Uchytil:** Conceptualization, Writing – original draft. **Thomas Loimer:** Formal analysis, Writing – review & editing.

Declaration of competing interest

The authors declare that they have no known competing financial interests or personal relationships that could have appeared to influence the work reported in this paper.

Data availability

Data will be made available on request.

Acknowledgments

Funding

This work was supported by AIC Androsch International Management Consulting GmbH, by Czech Science Foundation project no. 19-23760J, and from ERDF/ESF project "UniQSurf — Centre of biointerfaces and hybrid functional materials" (No. CZ.02.1.01/0.0/0.0/17_048/0007411). The authors acknowledge TU Wien Bibliothek for financial support through its Open Access Funding Programme.

References

[1] J. Caro, Hierarchy in inorganic membranes, Chem. Soc. Rev. 45 (2016) 3468–3478, http://dx.doi.org/10.1039/C5CS00597C.
[2] E.A. Mason, A. Malinauskas, Gas Transport in Porous Media: The Dusty-Gas Model, Elsevier, 1983.
[3] P. Uchytil, Gas permeation in ceramic membranes Part I. Theory and testing of ceramic membranes, J. Membr. Sci. 97 (1994) 139–144, http://dx.doi.org/10.1016/0376-7388(94)00156-S.
[4] S. Thomas, R. Schäfer, J. Caro, A. Seidel-Morgenstern, Investigation of mass transfer through inorganic membranes with several layers, Catal. Today 67 (1–3) (2001) 205–216, http://dx.doi.org/10.1016/S0920-5861(01)00288-7.
[5] P. Uchytil, Z. Brož, Gas permeation in ceramic membranes Part II. Modeling of gas permeation through ceramic membrane with one supported layer, J. Membr. Sci. 97 (1994) 145–153, http://dx.doi.org/10.1016/0376-7388(94)00157-T.
[6] P. Uchytil, Pore-size determination in the separation layer of a ceramic membrane using the permeation method, J. Mater. Sci. 31 (23) (1996) 6293–6298, http://dx.doi.org/10.1007/BF00354452.
[7] P. Uchytil, O. Schramm, A. Seidel-Morgenstern, Influence of the transport direction on gas permeation in two-layer ceramic membranes, J. Membr. Sci. 170 (2) (2000) 215–224, http://dx.doi.org/10.1016/S0376-7388(99)00370-1.
[8] V. Roldughin, V. Zhdanov, E. Sherysheva, The effect of gas surface diffusion on the asymmetric permeability of two-layer porous membranes, Colloid J. 74 (6) (2012) 717–720, http://dx.doi.org/10.1134/S1061933X12060129.
[9] F. Kapteijn, X. Wang, Zeolite membranes – The importance of support analysis, Chem. Ing. Tech. 94 (1–2) (2022) 23–30, http://dx.doi.org/10.1002/cite.202100136.
[10] H. Rhim, S.-T. Hwang, Transport of capillary condensate, J. Colloid Interface Sci. 52 (1975) 174–181, http://dx.doi.org/10.1016/0021-9797(75)90314-8.
[11] K.-H. Lee, S.-T. Hwang, The transport of condensible vapors through a microporous vycor glass membrane, J. Colloid Interface Sci. 110 (2) (1986) 544–555, http://dx.doi.org/10.1016/0021-9797(86)90407-8.
[12] R.J.R. Uhlhorn, K. Keizer, A.J. Burggraaf, Gas transport and separation with ceramic membranes. Part I. Multilayer diffusion and capillary condensation, J. Membr. Sci. 66 (2–3) (1992) 259–269, http://dx.doi.org/10.1016/0376-7388(92)87016-Q.

[13] P. Uchytil, R. Petrickovic, S. Thomas, A. Seidel-Morgenstern, Influence of capillary condensation effects on mass transport through porous membranes, Sep. Purif. Technol. 33 (3) (2003) 273–281, http://dx.doi.org/10.1016/S1383-5866(03)00087-X.

[14] P. Uchytil, R. Petrickovic, A. Seidel-Morgenstern, Study of capillary condensation of butane in a vycor glass membrane, J. Membr. Sci. 264 (1–2) (2005) 27–36, http://dx.doi.org/10.1016/j.memsci.2005.04.017.

[15] P. Uchytil, R. Petrickovic, A. Seidel-Morgenstern, Transport of butane in a porous vycor glass membrane in the region of condensation pressure, J. Membr. Sci. 293 (1–2) (2007) 15–21, http://dx.doi.org/10.1016/j.memsci.2007.01.020.

[16] A. Rathi, E.S. Kikkinides, D.M. Ford, P.A. Monson, Nonequilibrium steady states in fluid transport through mesopores: Dynamic mean field theory and nonequilibrium molecular dynamics, Langmuir 35 (17) (2019) 5702–5710, http://dx.doi.org/10.1021/acs.langmuir.9b00112.

[17] W. Schneider, Vapor flow through a porous membrane — a throttling process with condensation and evaporation, Acta Mech. 47 (1) (1983) 15–25, http://dx.doi.org/10.1007/BF01176497.

[18] G. Hohenbichler, A. Köppl, W. Schneider, Evaporation of a liquid flowing through a slender porous cylinder, Acta Mech. 107 (1994) 21–32, http://dx.doi.org/10.1007/BF01201817.

[19] T. Loimer, P. Uchytil, R. Petrickovic, K. Setnickova, The flow of butane and isobutane vapors near saturation through porous vycor glass membranes, J. Membr. Sci. 383 (2011) 104–115, http://dx.doi.org/10.1016/j.memsci.2011.08.035.

[20] P. Uchytil, T. Loimer, Large mass flux differences for opposite flow directions of a condensable gas through an asymmetric porous membrane, J. Membr. Sci. 470 (2014) 451–457, http://dx.doi.org/10.1016/j.memsci.2014.07.055.

[21] T. Loimer, P. Uchytil, Influence of the flow direction on the mass transport of vapors through membranes consisting of several layers, Exp. Therm Fluid Sci. 67 (2015) 2–5, http://dx.doi.org/10.1016/j.expthermflusci.2014.12.012.

[22] P. Uchytil, J. Reznickova, K. Setnickova, T. Loimer, Comparison of the flow of permanent and condensable gases through an asymmetric porous membrane, Chem. Ing. Tech. 88 (11) (2016) 1779–1787, http://dx.doi.org/10.1002/cite.201600047.

[23] VDI-Gesellschaft Verfahrenstechnik und Chemieingenieurwesen (Ed.), VDI Heat Atlas, second ed., Springer, 2010, http://dx.doi.org/10.1007/978-3-540-77877-6.

[24] J. Dykyj, J. Svoboda, R.C. Wilhoit, M. Frenkel, K.R. Hall, Vapor pressure and antoine constants for hydrocarbon, and sulfur, selenium, tellurium, and halogen containing organic compounds, in: K.R. Hall (Ed.), Vapor Pressure of Chemicals, in: LandOlt-BÖrnstein. New Series, Group IV: Physical Chemistry, 20A, Springer, 1999.

[25] R.C. Wilhoit, K.N. Marsh, X. Hong, N. Gadalla, M. Frenkel, Densities of aliphatic hydrocarbon: Alkanes, in: M. Frenkel, K.R. Hall, K.N. Marsh (Eds.), Thermodynamic Properties of Organic Compounds and their Mixtures, in: Landolt-Börnstein. New Series, Group IV: Physical Chemistry, vol. 8B, Springer, 1996.

[26] J.H. Dymond, K.N. Marsh, R.C. Wilhoit, K.C. Wong, Virial coefficients of pure gases, in: K. N. Marsh M. Frenkel (Ed.), Virial Coefficients of Pure Gases and Mixtures, in: Landolt-Börnstein. New Series, Group IV: Physical Chemistry, vol. 21A, Springer, 2002.

[27] R.H. Perry, D.W. Green, J.O. Maloney, Perry's Chemical Engineers' Handbook, seventh ed., McGraw-Hill, 1997.

[28] T.E. Daubert, R.P. Danner, Physical and Thermodynamic Properties of Pure Chemicals – Data Compilation, Taylor and Francis, Washington D.C, 1989-1994.

[29] VDI-Gesellschaft Verfahrenstechnik und Chemieingenieurwesen (Ed.), VDI-WÄrmeatlas, ninth ed., VDI-Verlag, Düsseldorf, 2002, http://dx.doi.org/10.1007/978-3-662-10743-0.

[30] C. Baroncini, P. Filippo, G. Latini, M. Pacetti, Organic liquid thermal conductivity: A prediction method in the reduced temperature range 0.3 to 0.8, Int. J. Thermophys. 2 (1) (1981) 21–38, http://dx.doi.org/10.1007/BF00503572.

[31] R.C. Reid, J.M. Prausnitz, B.E. Poling, The Properties of Gases and Liquids, fourth ed., McGraw-Hill, 1987.

[32] K. Stephan, H. Hildwein, Recommended Data of Selected Compounds and Binary Mixtures, in: Chemistry Data Series, vol. 4 | 1+2, DECHEMA, Frankfurt am Main, 1987.

[33] R.W. Cannon, E. Gugel, G. Leimer, G. Woetting, R.B. Heimann, Ceramics, advanced structural products, in: Ullmann's Encyclopedia of Industrial Chemistry, Wiley-VCH, 2011, http://dx.doi.org/10.1002/14356007.a06_043.pub2.

[34] A.E. Scheidegger, The Physics of Flow Through Porous Media, third ed., University of Toronto Press, 1974.

[35] J.K. Carson, S.J. Lovatt, D.J. Tanner, A.C. Cleland, Thermal conductivity bounds for isotropic, porous materials, Int. J. Heat Mass Transfer 48 (11) (2005) 2150–2158, http://dx.doi.org/10.1016/j.ijheatmasstransfer.2004.12.032.

[36] MATLAB Release 2017a, The MathWorks, Inc., Natick, Massachusetts, United States, 2017.

[37] H. Verweij, Inorganic membranes, Curr. Opin. Chem. Eng. 1 (2) (2012) 156–162, http://dx.doi.org/10.1016/j.coche.2012.03.006.

[38] W. Rasband, ImageJ Version 1.50, National Institute of Mental Health, Bethesda, Maryland, United States, 2017, URL https://imagej.nih.gov/ij.